PCCP

Accepted Manuscript

ROYAL SOCIETY OF CHEMISTRY

www.rsc.org/pccp

Modeling Ultrafast Exciton Deactivation in Oligothiophenes *via* Nonadiabatic Dynamics

Daniele Fazzi, Mario Barbatti, Walter Thiel

Max-Planck-Institut für Kohlenforschung, Kaiser-Wilhelm-Platz 1, D-45470 Mülheim an der Ruhr (Germany)

KEYWORDS

nonadiabatic excited-state dynamics, oligothiophenes, ultrafast processes, photophysics, organic photovoltaics.

ABSTRACT

Ultrafast excited-state processes play a key role in organic electronics and photovoltaics, governing the way on how excitons can relax and separate. Through the use of nonadiabatic excited-state dynamics, relaxation processes were investigated at the sub-picosecond timescale in thiophene and oligothiophenes (*n*T, *n* = 2,3,4), prototype oligomers for efficient π-electron conjugated polymers adopted in photovoltaics. For thiophene, TDDFT and TDA nonadiabatic excited-state dynamics revealed ultrafast nonradiative relaxation processes through ring opening and ring puckering, bringing the system to an S_1/S_0 conical intersection seam. The computed relaxation time is 110 fs, matching well the experimental one (~105 fs). In oligothiophenes (*n* = 2-4), high-energy (*hot*) excitations were considered. Exciton relaxation through the manifold of excited states to the lowest excited state is predicted to occur within ~150-200 fs, involving bond stretching, ring puckering, and torsional oscillations. For the longer oligomer (*4*T), the ultrafast relaxation process leads to exciton localization over three thiophene rings in 150 fs. These data agree with the self-localization mechanism (~100-200 fs) observed for poly(3-hexylthiophene) (P3HT) and shed light on the complex exciton relaxation dynamics occurring in π-conjugated oligomers of potential interest for optoelectronic applications.

1 INTRODUCTION

Photovoltaics has assumed a primary role in the last decades, representing a reliable, clean, and renewable way to produce energy from sunlight.[1] In this frame, organic π-electron conjugated materials, in the form of small molecules, polymers, or molecular aggregates,[2] became attractive candidates for photovoltaic applications,[3] along with other classes of materials such as amorphous silicon,[4] dye-sensitized systems,[5] and perovskites.[6-8]

In organic photovoltaics (OPV), the device is prepared as a blend of two materials, an optically-active electron donor (D) and an electron acceptor (A). Light is absorbed by the optically-active material creating a photoexcited species, usually referred as exciton (i.e. a bound electron-hole pair). The exciton, in a simple picture, diffuses through the material, the charges are then separated at the donor-acceptor (D-A) interface, and finally they are collected at electrodes.[1, 9] In these basic steps of light-to-current production, the bottleneck in OPV efficiency consists of the ability to separate the photoinitiated electron-hole species[10] and to avoid any kind of dissipative channels, like excited-state internal conversion or charge recombination.[11] For this reason, ultrafast photoinduced deactivation processes play a key role in OPV, determining the fate of the early photoexcited species and how the energy will be released, redistributed, and transferred.[12-15]

High-resolution ultrafast transient absorption spectroscopy (e.g. pump-probe or pump-push-probe techniques)[16] revealed that for π-conjugated molecules and polymers, exciton relaxation to the lowest excited state occurs within tens to hundreds of femtoseconds, evolving from delocalized states toward more localized ones.[17-19] For instance, in P3HT (poly(3-hexylthiophene)), one of the most studied, best performing OPV materials amongst *homo*-polymers, the majority of the Stokes shift and anisotropy decay in solution or film happens in the first 200 fs.[17, 20] This means that in P3HT ultrafast exciton dynamics, from an extended delocalized excited state to a state localized over few monomers,[21, 22] occurs within the first hundreds of femtoseconds. Similar dynamics were observed for the last generation of OPV polymeric materials, giving power conversion efficiencies (PCE) up to 13%.[23] Compounds better known by the acronyms PCDTBT,[24] PCPDTBT,[19] and PBDTTPD[25] are examples of such efficient D-A copolymers. All of them undergo ultrafast excited-state relaxation,[26-28] recovering the Stokes shift in the first 200 fs both in solution and in solid-state films.

A variety of parameters affect the excited-state dynamics, such as excitation energies, solvent, molecular aggregation, and morphology of the films.[17] In any case,

however, the typical time-scales for the initial relaxation dynamics are observed to be hundreds of femtoseconds.[18, 21, 29, 30] Also for D-A bulk heterojunction solar cells, regardless of the organic materials (small molecules, *homo*- or *co*-polymers) used as donor, it has been generally found that the initial excited-state dynamics and charge-transfer process occurs in 100-200 fs.[31-33]

At this stage, it is highly desirable to strengthen the understanding of the basic relaxation processes[34, 35] underlying the ultrafast exciton deactivation in organic π-conjugated materials,[11, 36-42] to help to make sense of all this accumulated empirical information.

Many insightful computational and theoretical investigations were published in the last years. Clark *et al.*[43] recently studied the femtosecond (100 fs) torsional relaxation mechanisms in oligofluorenes (oligomers of interest for OPV, light emitting diodes, and photonic applications) *via* combined transient absorption spectroscopy and nonadiabatic molecular dynamics simulations. They were able to elucidate the ultrafast transitions from S_n (high-energy singlet excited states) to S_1 through a series of nonadiabatic events in which the system undergoes ultrafast conformational (torsional) changes.

Nelson *et al.*[44] applied nonadiabatic excited-state molecular dynamics to a series of interesting materials for OPV applications, such as oligomers of poly-(phenylene ethylene) (PPV),[45] poly-(phenylene ethynylene) (PPE),[46] and the donor p-DTS(PTTh$_2$)$_2$, the latter featuring the record high of 6.7% PCE amongst small molecules.[47] Their methodology combines the fewest-switches surface hopping (FSSH) approach[48] with excited-state calculations using the collective electronic oscillator method at the configuration interaction singles (CIS) level based on the semiempirical AM1 model Hamiltonian.[49] They demonstrated that the redistribution of the excess electronic energy occurs on the femtosecond time scale, involving vibrational degrees of freedom coupled to the electronic system.

Prezhdo *et al.*[50-54] developed an efficient methodology for surface hopping dynamics based on single-determinant DFT[55] and applied it to study exciton and charge transfer dynamics in organic/organic interfaces,[54] carbon naonotubes,[50] and hybrid materials.[56] For the case of the P3HT polymer/carbon nanotube interface, they found an asymmetry in the electron and hole dynamics, with the first one being orders of magnitude faster than the latter.[57]

Tamura *et al.*[12-14, 58] investigated the ultrafast charge separation in P3HT/C_{60}, showing that efficient charge separation is enhanced by electron delocalization and high-energy excitation.[12, 13] Dynamics were carried out using the multiconfiguration time-dependent Hartree (MCTDH) method, based on a linear vibronic coupling (LVC) model.[14]

In the current work, we use surface hopping based on time-dependent density functional theory (TDDFT) and the Tamm-Dancoff approximation (TDA) to investigate the exciton relaxation dynamics and their typical time scales in oligothiophenes. Oligothiophenes, although well known since decades for their optoelectronic properties,[59-61] still represent the best model for studying more interesting and efficient materials like P3HT[10] or thiophene-based polymers used nowadays in OPV applications.[3] Furthermore, there is still not yet a complete physical-chemical understanding regarding their ultrafast (~50-200 fs) excited-state deactivation mechanisms.

We investigated four different species, systematically increasing their size (Scheme 1) from a single thiophene ring (*1*T) up to oligomers with four rings (*4*T). The effects of electron delocalization upon the exciton relaxation dynamics were explored considering both low- and high-energy excitations.[20]

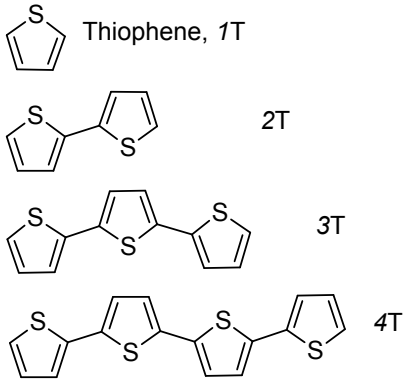

Scheme 1.

The basic questions we want to address are: which are the main excited-state deactivation mechanisms in oligothiophenes? What is the effect of the π-electron conjugation length on the internal deactivation processes and on the time scales? Which is the typical relaxation time scale after high-energy excitation?

As background to these physical-chemical investigations, we have performed a systematic methodological search concerning the computational parameters for thiophene to identify the most adequate, yet affordable, DFT functionals, basis sets, and methods (TDDFT *vs.* TDA). Complementary to a recent benchmark published by our group,[62] these are results of interest in their own right for computational chemists, which will be presented and validated against experimental data and multireference results from literature.

2 METHODS

Ground- and excited-state properties of oligothiophenes *n*T, with *n* = *1-4*, were investigated with DFT. Absorption cross sections were computed with the nuclear ensemble method based on harmonic oscillator Wigner distributions.[63] Diverse computational methods and levels were considered in these simulations. They are specified in Table 1.

Table 1: Characterization of method, computational level, number of points (N_p), number of excited states (N_{fs}), and phenomenological broadening (δ) in the simulation of absorption spectra.

*n*T	Method	Functional	Basis set	N_p	N_{fs}	δ(eV)
*1*T	TDDFT	ωB97XD[64]	6-31G*	300	10	0.05
*1*T	TDDFT	ωB97XD	6-311+G*	300	15	0.05
*1*T	TDA	ωB97XD	6-31G*	300	10	0.05
*1*T	TDA	ωB97XD	6-311+G*	300	15	0.05
*1*T	TDDFT	B3LYP[65, 66]	6-31G*	300	10	0.05
*1*T	TDDFT	B3LYP	6-311+G*	300	16	0.05
*1*T	TDA	B3LYP	6-31G*	300	10	0.05
*1*T	TDA	B3LYP	6-311+G*	300	18	0.05
*2*T	TDDFT	ωB97XD	6-31G*	300	10	0.05
*2*T	TDDFT	ωB97XD	6-311+G*	300	15	0.05
*2*T	TDDFT	PBE0[67]	6-311+G*	300	19	0.05
*2*T	TDDFT	CAM-B3LYP[68]	6-311+G*	300	10	0.05
*3*T	TDDFT	ωB97XD	6-31G*	300	10	0.05
*3*T	TDDFT	ωB97XD	6-311+G*	300	11	0.05
*4*T	TDDFT	ωB97XD	6-31G*	300	15	0.05
*4*T	TDDFT	ωB97XD	6-311+G*	300	12	0.05

Nonadiabatic excited-state dynamics[69-71] were done with TDDFT (and also TDA[69] for *1*T) using the FSSH method[48] as implemented in NEWTON-X[72, 73] interfaced with Gaussian 09.[74] The time step for integration of the classical equations was 0.5 fs. The integration of the quantum equations was done with 0.025 fs steps using interpolated properties between classical steps. Time-dependent coefficients were corrected for

decoherence effects as described in Ref.[75] Nonadiabatic couplings between excited states were computed by finite differences.[76-78] Due to the limitations of the linear-response TDDFT and Kohn-Sham DFT to provide reliable electronic states near intersections with the ground state,[76] nonadiabatic transitions between the excited and the ground states were not computed. Trajectories ran for a maximum of 300 fs or until a crossing with the ground state (within 0.1 eV) was reached. In such cases, the last time step was taken as an indication of internal conversion to the ground state.[79] Under this assumption, the occupation of the ground state (n_0), at each time step, was computed as: $n_0 = \left(n_{hops}/N_{traj}\right) \cdot n_1'$, with $\left(n_{hops}/N_{traj}\right)$ the number of S_1/S_0 *hops* over the total number of trajectories and n_1' the occupation (fraction of trajectories) of S_1 before the transition, as given by the FSSH algorithm. To compensate the transfer to S_0, the S_1 occupation was corrected to $n_1 = \left(1 - n_{hops}/N_{traj}\right) \cdot n_1'$. The occupations of all other states were given by the FSSH algorithm as usual.

Several sets of dynamics simulations were run, with different computational setups. They are described in Table 2. Initial conditions were selected from the simulated spectra at the same level, from within narrow spectral windows. Because different adiabatic states may contribute to the same spectral window, the number of trajectories starting in each state was determined by a stochastic algorithm sampling the points of the Wigner distribution according to their oscillator strengths. Thus, for instance, dynamics of *1*T simulated with TDDFT/ωB97XD/6-31G* (see Table 2) started at 6.0 ± 0.5 eV, with 171 trajectories initially in S_1 and 118 in S_2.

Table 2: Characterization of method, computational level, total number of trajectories, initial number of trajectories in each state, initial spectral window, and number of states considered for each set of dynamics simulations.

*n*T	Method	Functional	Basis set	Total Trajs.	Starting state S_1, S_2, S_3, …	Spectral window (eV)	Number of states
*1*T	TDDFT	ωB97XD	6-31G*	289	171, 118	6.0 ± 0.5	3
*1*T	TDDFT	ωB97XD	6-311+G*	293	186, 107	6.0 ± 0.5	3
*1*T	TDA	ωB97XD	6-31G*	208	113, 95	6.2 ± 0.5	3
*1*T	TDA	ωB97XD	6-311+G*	118	67, 51	6.0 ± 0.5	3
*1*T	TDDFT	B3LYP	6-31G*	301	159, 142	5.75 ± 0.5	3
*1*T	TDA	B3LYP	6-31G*	138	43, 48, 47	5.75 ± 0.5	4
*2*T	TDDFT	ωB97XD	6-31G*	40	40	4.5 ± 0.2	2
*2*T	TDDFT	ωB97XD	6-31G*	44	2, 7, 13, 10, 9, 2	5.5 ± 0.5	7
*2*T	TDDFT	PBE0[a]	SVP	70	70	4.2 ± 0.2	2
*2*T	TDDFT	PBE0[a]	SVP	42	0,0,42	5.4 ± 0.2	3
*3*T	TDDFT	ωB97XD	6-31G*	39	0, 1, 6, 8, 8, 16	5.6 ± 0.5	7
*4*T	TDDFT	ωB97XD	6-31G*	14	14 in S_{11}	5.5 ± 0.5	12

[a] In this case, NEWTON-X interfaced with TURBOMOLE[80] has been used.

3 RESULTS AND DISCUSSION

3.1 Ultrafast deactivation mechanisms for thiophene

The excited states and ultrafast deactivation mechanisms for thiophene have been extensively investigated in the past years. Seminal theoretical and computational works using DFT (TDDFT, DFT/MRCI), coupled cluster methods (CC2, CCSD and CCSDR(3)), and multireference (CASPT2) methods have been reported by Marian *et al.*,[81-84] Stenrup *et al.*,[85] and Fang *et al.*[86] Absorption bands in the gas-phase electronic spectrum have been attributed to two low-lying absorbing singlet states featuring π–π^* character.[87] Time-resolved pump-probe femtosecond multiphoton ionization spectroscopy revealed the presence of ultrafast relaxation dynamics (*via* nonradiative decays) after photoexcitation.[83] Thiophene is in fact a nonfluorescent molecule and a possible mechanism proposed for excited-state relaxation involves an ultrafast decay (~80 ± 10 fs) of the initial wavepacket to the low-lying excited states, followed by a subsequent fast decay (~25 ± 10 fs) *via* a conical intersection (i.e. ring opening) to S_0.[83]

Potential energy profiles computed at the TDDFT//DFT/MRCI and MS-CASPT2 levels provided the energies and geometries of the excited-state minima (puckered configuration) and the S_1/S_0 conical intersection (ring opening).[82, 85] Nonadiabatic excited-state dynamics at the CASSCF level,[86] covering only the first singlet excited state, predicted an ultrafast decay to the ground state *via* a ring opening conical intersection, with an averaged time constant of 65 ± 5 fs. However, this study ignored the fact that two close-lying singlet excited states (S_1 and S_2) are concomitantly photoexcited by the pump laser, which limits the validity of the results.

Here, we report TDDFT and TDA nonadiabatic excited-state dynamics of *1*T, which for the first time considers *both* the S_1 and S_2 states.

3.1.1 *1*T: Absorption spectrum, minima, and potential energy profiles

As the starting point for the investigation, absorption spectra were calculated via the nuclear ensemble method. Figure 1 shows the TDDFT *vs.* TDA spectra for two different functionals (ωB97XD *vs* B3LYP) and basis sets (6-31G* and 6-311+G*). The contributions of the $S_0 \rightarrow S_1$ and $S_0 \rightarrow S_2$ transitions to the first absorption band are reported in black and grey, respectively.

In both TDDFT and TDA methods, the basis set choice strongly affects the intensity ratio between the first (5.0-6.5 eV) and the second absorption (~6.5-8 eV) bands and the energy range of the latter. An extended basis set (6-311+G*) increases the global cross section of the second band without affecting, in terms of spectral range and intensity, the first band. The first absorption band consists of a convolution of two absorptions, $S_0 \rightarrow S_1$ (black line in Figure 1) and $S_0 \rightarrow S_2$ (grey line), both characterized by π–π^* transitions (see Table 3 and Supplementary Data, Section S1). Because of their overlap and vicinity, both S_1 and S_2 excited states have to be considered in the nonadiabatic dynamics investigation.

For the larger basis set, the computed TDDFT absorption spectra *quantitatively* reproduce the experimental gas phase spectrum,[87] see Figure 1. Generally, ωB97XD overestimates the energy of the second absorption band, while B3LYP nicely agrees with the experimental spectrum. TDA, in turn, overestimates the vertical transition energies by ~0.2-0.3 eV with respect to TDDFT (Table 3 and Figure 1).

The comparison between B3LYP and the measurements does not cover the relative energies of dark states that do not show up in the spectrum. ωB97XD should provide a better balanced description of all kinds of states; this is confirmed by the superior results for the dynamics obtained with the latter functional (see Section 3.1.2). In Ref. [88], structural and electronic properties in oligothiophenes with up to 20 rings were investigated with different functionals. It was shown that ωB97XD is one of the functionals with the lowest error in predicting quantities like ionization potentials, bond length alternations, and electronic transitions in neutral and charged species, while B3LYP usually tends to underestimate the values for the longer chain lengths.

Table 3: TDDFT and TDA vertical transition energies for S_1 and S_2 states in *1*T. ωB97XD and B3LYP with 6-31G* and 6-311+G* basis sets are compared. The energy (E), the oscillator strength (f), and the main molecular orbitals involved in the transitions (CI) are reported.

		S_1			S_2		
		E (eV)	f	CI	E (eV)	f	CI
TDDFT ωB97XD	6-31G*	6.09	0.0912	H – L	6.18	0.1008	H-1 – L H – L+1
	6-311+G*	5.91	0.1044	H – L	6.02	0.1075	H-1 – L H – L+7
TDA ωB97XD	6-31G*	6.33	0.1105	H-1 – L H – L+2	6.44	0.1237	H – L H-2 – L+1
	6-311+G*	6.16	0.1152	H-1 – L H – L+7	6.22	0.1402	H – L H-1 – L+7

TDDFT B3LYP	6-31G*	5.92	0.0869	H – L	5.99	0.0816	H-1 – L H – L+2
	6-311+G*	5.71	0.0993	H – L	5.81	0.0865	H-1 – L H – L+6
TDA B3LYP	6-31G*[a]	6.13	0.0892	H-1 – L H – L+2	6.28	0.1182	H – L H-2 – L+1
	6-311+G*[a]	5.93	0.0919	H-1 – L H – L+6	6.02	0.1339	H - L H-1 – L+6

[a] For the case of TDA-B3LYP/6-31G*, the reported states are S_2 (6.13 eV) and S_3 (6.28 eV). S_1 (6.07 eV) is dark (f = 0.0003). For TDA-B3LYP/6-311+G*, the states reported are S_2 (5.93 eV) and S_4 (6.02 eV).

Minima of excited states were computed at the TDDFT level (see equilibrium geometries in the Supplementary Data, Section S2). The equilibrium structures have nonplanar puckered or ring opening geometries, as also obtained in previous TDDFT and MS-CASPT2 simulations.[82, 85] In the puckered structures, sulfur is out of the ring plane and the TDDFT computed degree of distortion is ~18°, while MS-CASPT2 predicts 27°.

Optimized potential energy profiles were computed as well at the TDDFT level (see Supplementary Data, Section S3), considering two reaction coordinates, namely the C-S stretching (ring opening) and the out-of-plane distortion (ring puckering). As already observed in DFT/MRCI and MS-CASPT2 calculations,[83, 85] the C-S elongation strongly destabilizes S_0 and stabilizes S_1, bringing the thiophene to a S_1/S_0 conical intersection.

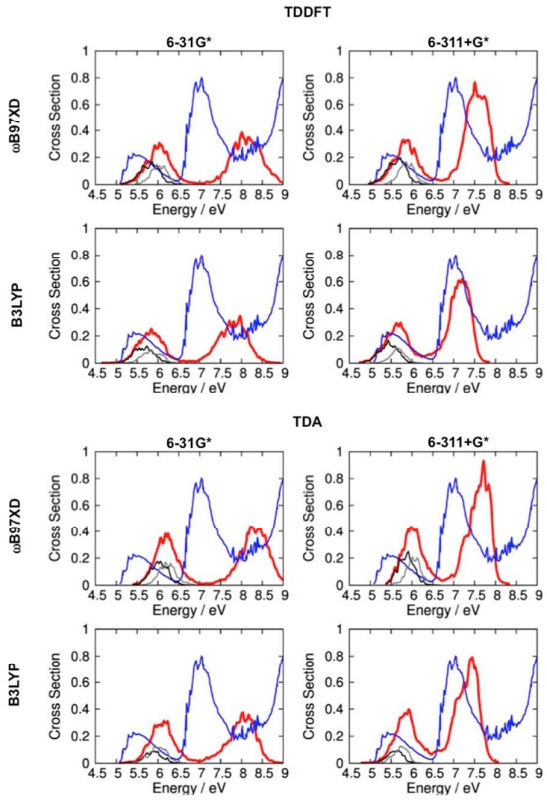

Figure 1. Absorption cross sections (in Å²/molecule) computed with the nuclear ensemble method. Results from different methods (TDDFT *vs.* TDA), functionals (ωB97XD *vs.* B3LYP), and basis sets (6-31G* *vs.* 6-311+G*) are compared. Black and grey lines represent the $S_0 \rightarrow S_1$ and $S_0 \rightarrow S_2$ absorption profiles. Gas-phase experimental spectrum (blue line) taken from Ref. [87]

3.1.2 *1*T: Nonadiabatic dynamics

Nonadiabatic excited-state dynamics runs were performed comparing TDDFT *vs.* TDA methods and ωB97XD *vs.* B3LYP functionals. Trajectories were initiated from the first absorption band, thus populating both S_1 and S_2 states. Dynamics with different basis sets (6-31G* and 6-311+G*) were tested as well, but no significant differences were found (see Supplementary Data, Section S4). For this reason, and to be consistent with the excited-state dynamics run for the oligothiophenes, we discuss only the 6-31G* data in the following.

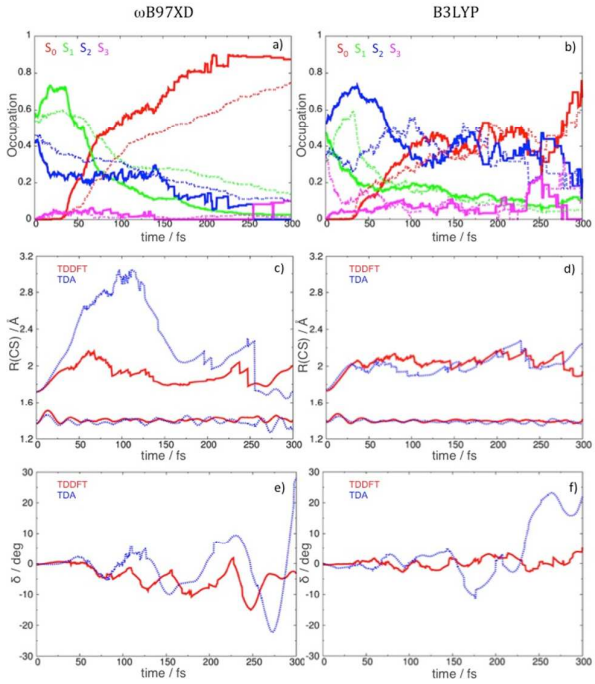

Figure 2. TDDFT *vs.* TDA nonadiabatic excited-state dynamics simulations. ωB97XD (left column), B3LYP (right column). Panels a) and b): occupation *vs.* time, solid lines: TDDFT, dashed lines: TDA. Panels c) and d): C-S bond lengths (R(CS)) *vs.* time. Panels e) and f): ring puckering angle (dihedral angle δ) *vs.* time. Red solid lines: TDDFT, blue dashed lines: TDA.

All combinations of methods and functions predict an ultrafast deactivation of the photoexcited species. Figure 2 (a and b) shows the occupation of the excited states as a function of time. Time constants for excited-state deactivation and ground-state population dynamics were derived through an exponential fitting in the case of ωB97XD. The same procedure was not applied to the B3LYP case, because the occupation of the electronic states *vs.* time is clearly non-exponential. These time constants and also those for the 6-311+G* basis set (Supplementary Data, Section S4) are given in Table 4.

According to the TDDFT-ωB97XD/6-31G* data, S_1 is populated in 80 fs, while S_0 is populated 30 fs later. These results nicely agree with the experiments,[83] which report first a vibrational relaxation to S_1 (τ_1 = 80 ± 10 fs) followed by internal conversion to the ground state (25 ± 10 fs). Although qualitatively correct, when computed with TDA-ωB97XD/6-31G*, τ_1 is somewhat larger than the experimental value. For TDDFT no significant basis set effect is observed, while for TDA basis set extension leads to a

smaller value for τ_1 (presumably reflecting some change in the excited-state potential energy surfaces). Further systematic studies would be necessary to fully investigate this effect.

Table 4: Exponential time constants for population of S_1 (τ_1) and of S_0 (τ_0). Experimental data from Ref. [83]

Method	Basis Set	τ_1 (fs)	τ_0 (fs)
TDDFT	6-31G*	80	30
TDA	6-31G*	185	18
TDDFT	6-311+G*	85	18
TDA	6-311+G*	135	20
Expt.		80	25

We analyzed the C-S bond lengths (both C-S bonds because they are not equivalent during the dynamics) and the puckering angle (defined as a C-C-C-S dihedral angle) along the trajectories. Results are reported in Figure 2 (c and d). For each method, in the first stage of the deactivation (~80 fs), a huge elongation of one C-S bond occurs, from ~1.75 Å to ~2.2 Å. For TDA (ωB97XD), the mean C-S distance reaches almost 3 Å. In this stage, the ring is almost flat (small out-of-plane distortion, Figure 2, e and f) and afterwards it starts to oscillate in a range up to 10°-20°. The computed average values of C-S elongations and ring puckering deformations, compared to the *static* potential energy profile calculations (see Supplementary Data, Section S3), match well the S_1/S_0 intersection geometries found for *1*T.[85]

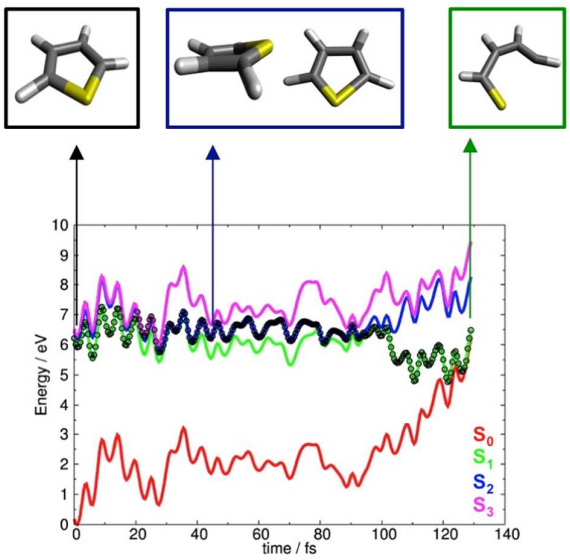

Figure 3. Time evolution of the excited-state energies for one representative trajectory (TD-ωB97XD/6-31G*). Snapshots of thiophene molecular structure along the dynamics (t = 0, 42, 130 fs). Black circles specify the currently occupied state in the dynamics.

In Figure 3 we show one representative trajectory from the TDDFT (ωB97XD) nonadiabatic excited-state dynamics. At t = 0, the thiophene ring is flat. At t = 42 fs, the ring puckering and C-S bond elongation start to occur (see central panel, lateral and top views). Around t = 100 fs, the energy difference between S_1 and S_0 drops below 0.8 eV and at t = 130 fs an S_1/S_0 intersection characterized by a ring opening occurs.

To briefly summarize this section, we computed TDDFT and TDA absorption spectra (including vibrational broadening) and nonadiabatic dynamics for thiophene. The dynamics simulations, making use of ωB97XD, reproduce the experimental data well. The deactivation mechanisms involve simultaneous ring opening and ring puckering on the 100 fs time scale.

3.2 Exciton dynamics after high-energy excitations in oligothiophenes

For the simulation of oligothiphenes, we considered only the ωB97XD functional for the evaluation of absorption spectra and excited-state dynamics. This was done because, first, the inclusion of dispersion interactions is necessary for long π-conjugated systems and interacting π-π systems[88, 89] and, second, the inclusion of range-separation corrections is needed to appropriately describe charge-transfer and Rydberg excited states in longer π-conjugated systems.[88]

In thiophene, fluorescence is completely quenched by nonradiative mechanisms involving singlet state deactivations (as discussed in the previous section). Upon increasing the number of thiophene rings, fluorescence turns on with high quantum yield.[90] In fact, oligothiophenes were extensively studied for their emissive properties (in solution or aggregates)[91-94] and used as organic light emitting diodes (OLED).[95]

By increasing the π-electron conjugation and the chain length, the quantum yield and the lifetime of the emitting state increase, which implies less efficient internal conversion from S_1 to S_0. For this reason, it is interesting to investigate the excited-state dynamics upon low- and high-energy photoexcitation, and to explore the decay mechanisms through the manifold of excited states.[49] Furthermore, high-energy excitation (also called *hot* excitation[32, 33]) has been demonstrated to be effective in

increasing the internal power conversion efficiency in bulk heterojunction OPV.[13, 32, 33] Therefore, a molecular understanding of the time-dependent effects, even for pristine oligomers/polymers, is urgent.

3.2.1 Spectrum simulations

In Figure 4 we report the TD-ωB97XD/6-31G* absorption spectra of *1*T, *2*T, *3*T, and *4*T. The spectrum of *1*T, also given in Figure 1, is shown here once more to make the comparison of the whole series easier. The experimental spectra of *2*T-*4*T were measured in dioxane,[92] while the spectrum of *1*T was recorded in the gas phase.[87] For *2*T-*4*T, the experimental cross sections shown in Figure 4 were divided by the refractive index of dioxane (n_r = 1.42) to compensate for solvent effects.[63]

The computed spectra well reproduce the experimental ones[90, 92] in terms of spectral energy, band intensity ratio, and band width. In a recent computational study, Improta *et al.*[96] claimed that the CAM-B3LYP and PBE0 functionals provide the best predictions for absorption and emission spectra of dithiophene (*2*T). In the Supplementary Data (see Section S5), we compare the re-computed (via nuclear ensemble method) CAM-B3LYP and PBE0 absorption spectra with the ωB97XD spectrum, showing the full validity and accuracy of the latter. A comparison of the spectra computed with the 6-31G* and 6-311+G* basis is provided in the Supplementary Data, Section S6. We also computed the vertical transition energies for the longest oligomer (*4*T) using B3LYP, see Supplementary Data (Section S6, Table S6.3). B3LYP predicts the vertical energy of the bright S_1 state at 2.9 eV, even lower than the experimental data. This strengthens the choice of the ωB97XD functional as the best compromise to describe both short and long π-conjugated systems.

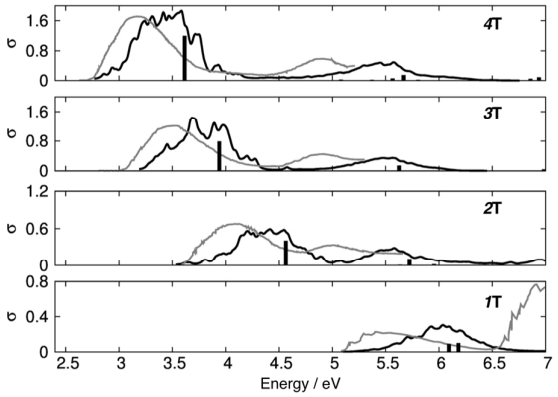

Figure 4. TDDFT (ωB97XD/6-31G*) absorption spectra (cross section, σ, in Å^2/molecule) from *1*T (bottom panel) to *4*T (upper panel). Sticks represent TDDFT vertical transition energies with heights proportional to their oscillator strengths. Experimental spectra (grey lines) taken from Ref. [87] (*1*T) and Ref. [92] (*2*T-*4*T).

The red shift of the low-energy band with increasing chain length and π-electron conjugation is well reproduced by ωB97XD. The high-energy band for oligothiophenes, centered at 5.5 eV, is blue-shifted by ~0.5 eV in comparison to the available experimental data[90] and, accordingly, it does not shift with the chain length as the low-energy band does. It is interesting to notice how much the origin of the low-energy band is red-shifted (~0.5-0.7 eV) with respect to the vertical transition, pointing to the importance of considering the simulation of the full band envelope for a correct prediction of the electronic spectrum. The electronic transitions belonging to both low- and high-energy bands have π–π* character. The molecular orbitals involved in the excitations are reported in the Supplementary Data, Section S1. Ground- and excited-state equilibrium geometries are also given in the Supplementary Data, Section S7.

3.2.2 Excited-state dynamics of *2*T

Trajectories were initiated from the low- and high-energy bands. The main results from TDDFT nonadiabatic excited-state dynamics of *2*T are collected in Figure 5.

Figure 5a shows the occupation for each electronic state, upon low- and high-energy excitations, in the 300 fs time window. The photophysics of *2*T differs extremely from that of *1*T: the π-electron conjugation between aromatic rings stabilizes the S_1 state, thus limiting the nonradiative channels between S_1 and S_0 when the first absorption band is photoexcited.[29]

When starting in the low-energy band (4.5 ± 0.2 eV) where only the S_1 state is populated (see Table 2), 35 out of 40 trajectories reached the maximum simulation time (300 fs) without crossing to the ground state. Only 5 trajectories stopped at a crossing with the ground state ($\Delta E(S_1\text{-}S_0) < 0.1$ eV). The occupation of S_1 at 300 fs is 80%, reflecting the reduction of S_1/S_0 nonradiative channels in the ultrafast time scale.

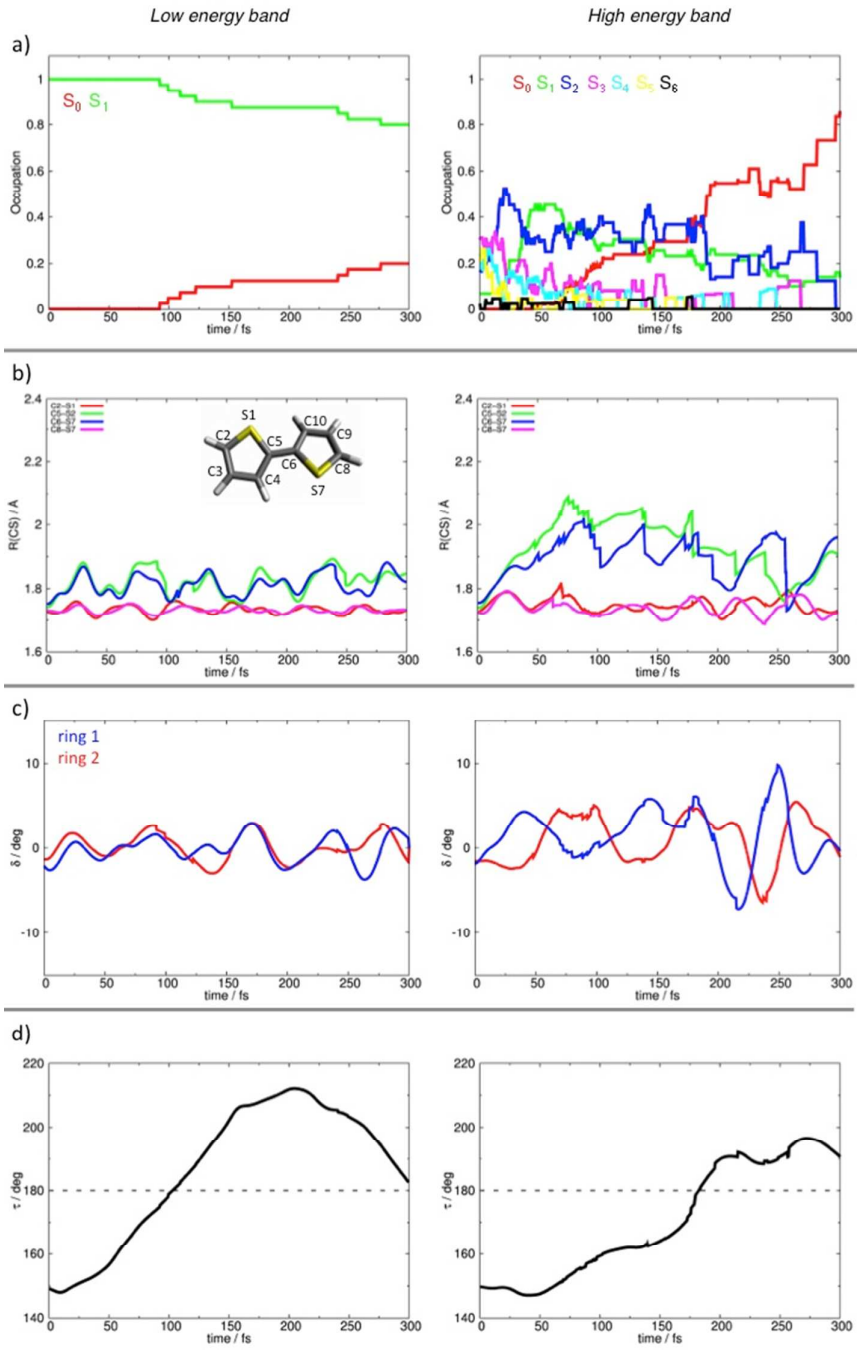

Figure 5. TDDFT (ωB97XD/6-31G*) nonadiabatic excited-state dynamics. Left(right) side, low(high)-energy band excitation. Panel a) Occupation of each electronic state investigated. Panel b) C-S bond elongation (R(CS)) *vs*. time. Molecular structure of *2*T, with atom labeling, shown as inset. Panel c) ring puckering (δ) *vs.* time; Panel d) torsional angle (τ) coordinate (S1-C5-C6-S7) *vs.* time.

By exciting the high-energy band (5.5 ± 0.5 eV), all states up to S_6 were populated, especially S_3 to S_5 (Table 2, Figure 5). 44 trajectories were propagated and 31 of them reached the S_1/S_0 crossing within 300 fs, namely 9 within 75 fs, 14 between 75 and 150 fs, and 8 after 225 fs. The remaining 13 did not reach the crossing with S_0 within the maximum simulation time. Thus, as expected, high-energy excitation increases the occurrence of nonradiative decay channels involving the S_1/S_0 crossing seam, leading to over 80% occupation of S_0 after 300 fs.

In the first 25 fs, ultrafast deactivation occurs and population is transferred to S_2 *via* nonadiabatic transitions. The S_1 occupation rises as well and reaches about 40% within 75 fs. From 75 to 175 fs, the occupation of high-lying excited states decreases nearly to zero and S_0 starts to be populated. Between 175 and 200 fs, the majority of the photoexcited population decays to S_0. At 300 fs, the S_1 occupation is less than 20%, with the remaining population transferred to S_0. Similarly to *1*T case, the deactivation mechanism involves large C-S bond deformations and ring puckering, and the conical intersection seam with the ground state is characterized by the ring opening of one thiophene (see Supplementary Data, Sections S8 and S9).

Figure 5b reports the C-S bond elongations along the dynamics started from both low- and high-energy bands. While in the low-energy case the C-S bond oscillations are limited between 1.7 to 1.9 Å, excitation in the high-energy band leads to trajectories with a higher kinetic energy that undergo larger oscillations (up to 2.1 Å), which contributes to dissipative processes. In particular, the inner C-S bonds (C1-S5 and C6-S7, Figure 5b) undergo strong variations, similar to those observed in *1*T (see Figure 2b). Huge C-S elongations occur in the first 75-80 fs (as in *1*T case), which is the time for transferring the photoexcited population from high-lying excited states to the S_2 and S_1 states. The excess kinetic energy is mostly transformed into deformation energy in terms of C-S stretching (see Supplementary Data, Section S10 for an example of a trajectory leading *2*T to the S_1/S_0 intersection seam through a ring opening mechanism).

Simultaneously, the two rings undergo puckering distortions (δ = C4-C3-C2-S1 and C10-C9-C8-S7, Figure 5c) and oscillations (stronger for the high-energy excitation than the low-energy band). We also monitored the torsional angle (τ) between the two thiophene rings along the dynamics (Figure 5d): τ oscillates passing through a flat conformation in ~100 fs when exciting the low-energy band, and in ~175 fs when exciting in the high-energy regime. It is worth noticing that fast oscillations, like C-S bond stretching and ring puckering, are more effective than the torsional ones in the dynamics of high-energy deactivation mechanisms. Indeed, they drive the majority of

the photoexcited population from S_n to low-lying excited states already in the first 75-100 fs, that is less than half of the period of the torsional oscillation.

Similar conclusions were obtained from TDDFT nonadiabatic excited-state dynamics computed at the PBE0/SVP level. The corresponding results for both low- and high-energy excitations are reported in the Supplementary Data (Section S11).

3.2.3 Excited-state dynamics of *3*T

Figure 6 shows the results of the nonadiabatic dynamics for *3*T upon high-energy excitation (5.5 eV band, Figure 4). As reported in Figure 6a, ultrafast deactivation of the photoexcited species occurs in the first 75 fs with subsequent occupation of S_1 (~40%), through a cascade of nonadiabatic transitions. Starting around 150 fs, the S_0 occupation rises, and at 300 fs the ground state is populated with an excess of 50%. From 39 trajectories generated, 4 reached a S_1/S_0 crossing within 75 fs, 12 within 150 fs, and 10 within 225 fs; 13 trajectories were still in the excited states at 300 fs. (See Supplementary Data, Section S12 for an example of a trajectory leading the system to the S_1/S_0 intersection seam through a ring opening mechanism and Section 9 for the corresponding potential energy profiles.)

We also monitored the C-S bond lengths (Figure 6b). Large elongations, from 1.7 up to 2 Å, occur in the inner ring in the first 75-100 fs, which is the time required to significantly populate S_1 (>50%). A flat conformation of *3*T is reached at 160 fs. Ultrafast bond oscillations (in particular C-S stretching) are responsible for the initial exciton relaxation. Torsional oscillations also occur on an ultrafast timescale, but they are not responsible for the initial excited-state deoccupation.

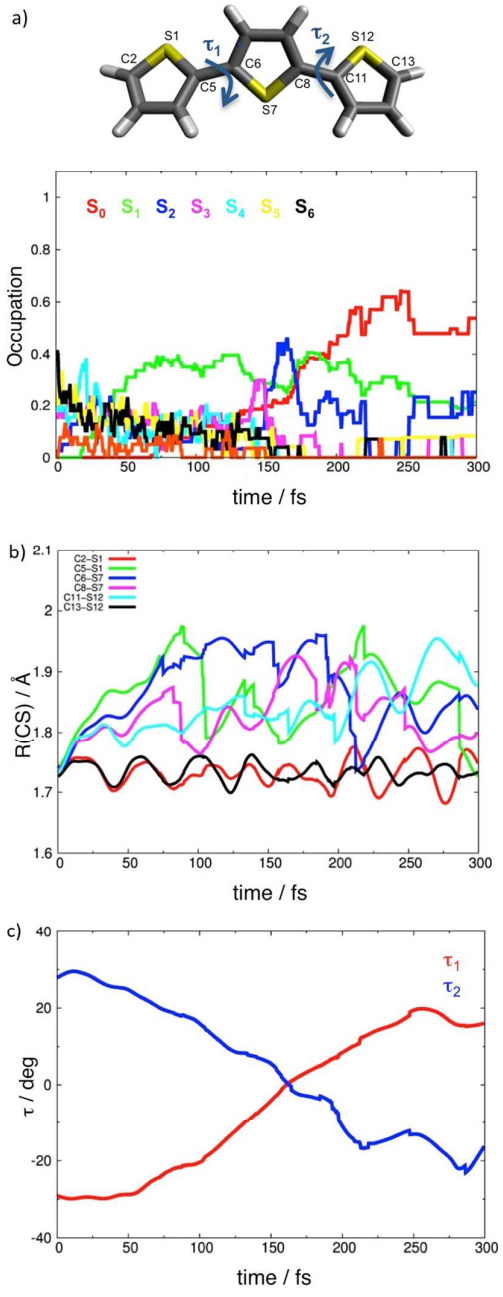

Figure 6. TDDFT (ωB97XD/6-31G*) nonadiabatic excited-state dynamics. Molecular structure of *3*T with atom labeling. Panel a) Occupation of each electronic state from high-energy band as function of time. Panel b) C-S bond elongations *vs.* time, Panel c) torsional angles (τ_1 and τ_2) *vs.* time.

3.2.4 Excited-state dynamics of *4*T

The 11 excited states needed to simulate the high-energy excitation of *4*T make it computationally very demanding to treat this oligomer with FSSH/TDDFT. For this reason, we simulated only few trajectories (N_{traj} = 14). In spite of this limitation, congruent trends can be recognized.

Figure 7a shows the occupation of all states. It is split into two parts due to the high number of excited states involved. We report the occupation of S_{12} to S_6 at the top and the occupation of S_5 to S_0 at the bottom. Similarly to the *2*T and *3*T cases, there is an ultrafast deactivation of the high-energy excited states within the first 50 fs. The occupation of the low-energy excited states (S_3, S_2, S_1) starts to increase after 75 fs. From 120 to 250 fs the occupation is almost constant, oscillating between S_2 and S_1. The ground state starts to be populated (>40%) within 270 fs. From 14 trajectories generated, 1 reached a S_1/S_0 crossing within 75 fs, 2 within 150 fs, 1 within 225 fs, and 10 were still in the excited states after 300 fs.

Looking at the oscillations of all C-S bonds, those belonging to the inner rings, C6-S7 (blue line in Figure 7b) and C8-S7 (pink line in Figure 7b), undergo larger deformations than the external ones. In particular, their maximum deformation of 2.0 Å is reached after around 150 fs when low-lying excited states (S_2 and S_1) are occupied to ~80%. The three dihedral angles oscillate mostly with the same period, and a flat conformation is reached between 125 and 225 fs.

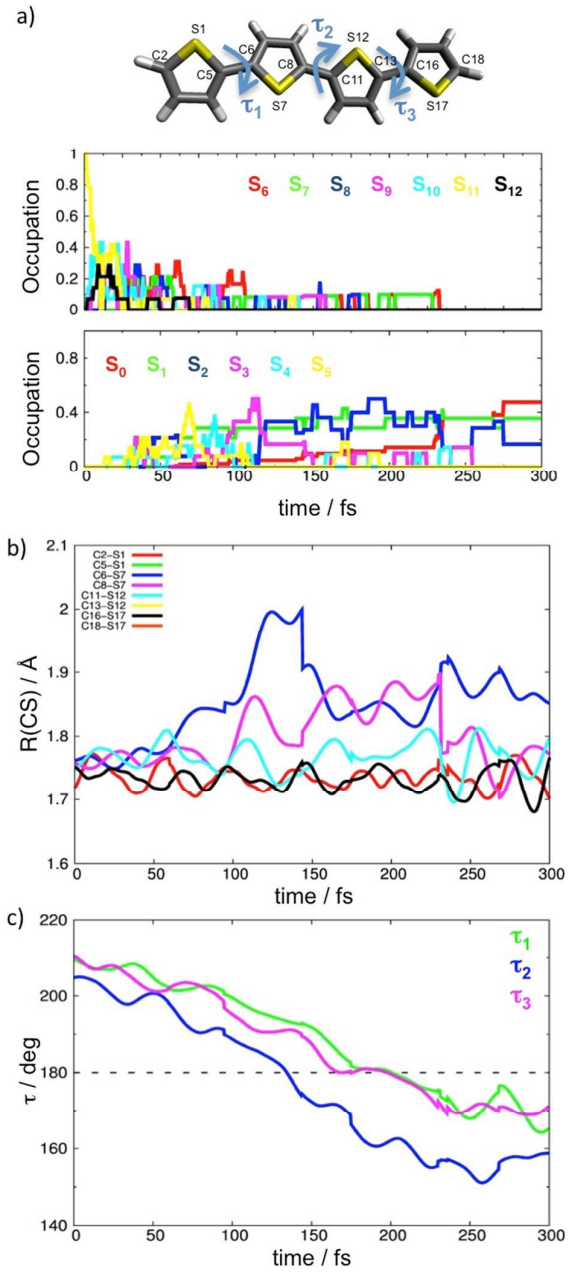

Figure 7. TDDFT (ωB97XD/6-31G*) nonadiabatic excited-state dynamics for *4*T. Panel a): occupation of each excited state from the high-energy band as function of time. Panel b): C-S bond elongations *vs.* time, Panel c): torsional angles (τ_1, τ_2, and τ_3) *vs.* time.

3.2.5 Exciton localization in oligothiophenes

To better understand the photophysics and exciton dynamics of oligothiophenes, we analyzed the electronic density difference between the excited states and the ground

state as a function of time for the longest oligomer (*4*T). This data is reported in Figure 8 for a representative trajectory. Electron-deficient regions are represented in orange and electron-rich regions are represented in green.

At t = 0, the photoexcited state (S_{11}) is completely *delocalized* over the four thiophene rings, with electron-rich density difference located on both inter-ring regions and on carbon-carbon ring bonds, featuring a quinoidal character.[97]

At t = 140 fs, the $S_2 \rightarrow S_1$ nonadiabatic transition occurs leading to a localization of the electronic density over three thiophene rings. This localization over three units is kept for the rest of the dynamics, until 300 fs.

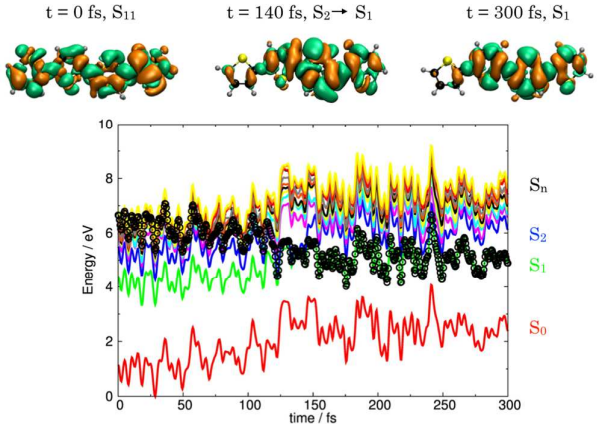

Figure 8. Snapshots of the electronic-density difference between the occupied excited state and the ground state for a representative *4*T trajectory. Orange regions are electron-poor, green are electron-rich. Bottom panel: time evolution of the excited-state energies for the trajectory considered in the analysis (TD-ωB97XD/6-31G*).

The process reflects well the experimental results from ultrafast transient absorption spectroscopy on long oligothiophenes or P3HT in solution,[20-22, 24] in which self-exciton localization over few aromatic units occurs in 200 fs.

Although *4*T is not representative for long oligothiophenes or polymers, such as P3HT (where ten units should be considered),[62, 98] we believe that the ultrafast exciton photophysics is already well captured and well described at this oligomer level.

4 CONCLUSIONS

The relaxation processes occurring on an ultrafast time scale for thiophene and oligothiophenes (*n*T) were investigated using nonadiabatic excited-state dynamics.

For the first time, TDDFT and TDA nonadiabatic excited-state dynamics were applied to study the photophysics of thiophene (*1*T). Competitive effects due to the photoexcitation of multiple low-lying excited states were taken into account. TDDFT quantitatively reproduces the absorption spectrum of *1*T and the ultrafast relaxation time scales, as probed by femtosecond photoelectron spectroscopy.[83]

Thiophene excited-state relaxation involves huge elongations of the CS bond, which drives the system to the S_1/S_0 intersection seam on an ultrafast timescale (~80 fs). The computed TDDFT decay time for the excited-state deactivation is 110 fs, while the experimental one is 105 fs.

Dynamics of high-energy photoexcitations were investigated with the aim of understanding the typical relaxation mechanisms and time scales in oligothiophenes.

In oligomers, π-electron delocalization stabilizes the system, limiting the access to non-radiative decay channels between S_1 and S_0 with increasing chain length. The fraction of trajectories in the excited states at 300 fs after high-energy excitation increases from 0.30 in *2*T to 0.33 in *3*T and to 0.71 in *4*T. This implies an elongation of the lifetime or a reduction of the S_1/S_0 internal-conversion probability or both.

Regardless of the oligomer length, photorelaxation to the lowest excited state takes place through a cascade of ultrafast nonadiabatic transfers amongst the manifold of excited states, within ~150-200 fs. Excited states relaxation processes are driven prevalently by fast motions, notably CS stretching and ring puckering deformations (70-100 fs).

For the longest oligomer considered here, *4*T, an exciton localization mechanism during the dynamics was observed. The initial photoexcited state is fully delocalized over four units and becomes localized over three units within 140 fs. Interestingly, the localization process occurs at the same time scale as experimentally observed for P3HT (~150-200 fs).[21, 22, 29]

As a general outcome, we conclude that the typical exciton relaxation decay time for thiophene-based materials (i.e. the time to populate S_1), upon high-energy excitations, is of the order of 150-200 fs. In the frame of photovoltaics, this implies that any exciton dissociation process has to happen on a time scale faster than 200 fs, as

recently observed in some polymer/fullerene[99] or polymer/oxide interfaces.[30] Only in this way is it possible to avoid inefficient mechanisms for light-to-current conversion (e.g. non-radiative decays or emission phenomena) and to raise the power conversion efficiency of organic solar cells.

ASSOCIATED CONTENT

Molecular orbitals involved in the main electronic transitions of *n*T. Optimized ground-state and excited-state equilibrium geometries of *n*T, *n* = 1-4. TDDFT absorption spectra and potential energy profiles (S_1 state) along CS and ring puckering coordinates for *n*T. TDDFT (ωB97XD/6-311+G*) nonadiabatic excited-state dynamics for *1*T. TDDFT (PBE0/SVP) nonadiabatic excited-state dynamics for *2*T.

AUTHOR INFORMATION

Corresponding authors:
fazzi@kofo.mpg.de;
barbatti@kofo.mpg.de;
thiel@kofo.mog.de

ACKNOWLEDGMENT

D. F. acknowledges the Alexander von Humboldt Foundation for supporting his research with a fellowship.

REFERENCES

1. D. B. Jean-Luc Brédas, Veaceslav Coropceanu, Jérôme Cornil, *Chemical Review*, 2004, 104, 4971-5003.
2. P. M. Beaujuge and J. M. Frechet, *Journal of the American Chemical Society*, 2011, 133, 20009-20029.
3. G. Li, R. Zhu and Y. Yang, *Nature Photonics*, 2012, 6, 153-161.
4. K. Sun, S. Shen, Y. Liang, P. E. Burrows, S. S. Mao and D. Wang, *Chemical Review*, 2014, 114, 8662-8719.
5. S. S. K. Raavi, P. Docampo, C. Wehrenfennig, M. J. P. Alcocer, G. Sadoughi, L. M. Herz, H. J. Snaith and A. Petrozza, *The Journal of Physical Chemistry C*, 2014, 118, 16825-16830.
6. F. De Angelis, *Account of Chemical Research*, 2014, 47, 3349-3360.

7. J. H. Heo, S. H. Im, J. H. Noh, T. N. Mandal, C.-S. Lim, J. A. Chang, Y. H. Lee, H.-j. Kim, A. Sarkar, M. K. Nazeeruddin, M. Grätzel and S. I. Seok, *Nature Photonics*, 2013, 7, 486-491.
8. S. D. Stranks, G. E. Eperon, G. Grancini, C. Menelaou, M. J. Alcocer, T. Leijtens, L. M. Herz, A. Petrozza and H. J. Snaith, *Science*, 2013, 342, 341-344.
9. J. E. N. Jean-Luc Brédas, Jérôm Cornil, Veaceslav Coropceanu, *Account of Chemical Research*, 2009, 42, 1691-1699.
10. F. Castet, G. D'Avino, L. Muccioli, J. Cornil and D. Beljonne, *Physical Chemistry Chemical Physics*, 2014, 16, 20279-20290.
11. J. D. Servaites, M. A. Ratner and T. J. Marks, *Energy & Environmental Science*, 2011, 4, 4410-4422.
12. H. Tamura and I. Burghardt, *The Journal of Physical Chemistry C*, 2013, 117, 15020-15025.
13. H. Tamura and I. Burghardt, *Journal of the American Chemical Society*, 2013, 135, 16364-16367.
14. H. Tamura, E. R. Bittner and I. Burghardt, *Journal of Chemical Physics.*, 2007, 126, 021103-021107.
15. G. Wu, Z. Li, X. Zhang and G. Lu, *The Journal of Physical Chemistry Letters*, 2014, 5, 2649-2656.
16. J. C.-G. Jenny Clark, Tersilla Virgili, Luca Bazzana, Guglielmo Lanzani, *Ultrafast Phenomena XVI Springer Series in Chemical Physics*, 2009, 42, 463-465.
17. N. Banerji, *Journal of Materials Chemistry C*, 2013, 1, 3052-3066.
18. N. Banerji, S. V. Bhosale, I. Petkova, S. J. Langford and E. Vauthey, *Physical Chemistry Chemical Physics*, 2011, 13, 1019-1029.
19. D. Fazzi, G. Grancini, M. Maiuri, D. Brida, G. Cerullo and G. Lanzani, *Physical Chemistry Chemical Physics*, 2012, 14, 6367-6374.
20. N. Banerji, S. Cowan, E. Vauthey and A. J. Heeger, *The Journal of Physical Chemistry C*, 2011, 115, 9726-9739.
21. E. Busby, E. C. Carroll, E. M. Chinn, L. Chang, A. J. Moulé and D. S. Larsen, *The Journal of Physical Chemistry Letters*, 2011, 2, 2764-2769.
22. P. C. Tapping and T. W. Kee, *The Journal of Physical Chemistry Letters*, 2014, 5, 1040-1047.
23. K. R. Graham, C. Cabanetos, J. P. Jahnke, M. N. Idso, A. El Labban, G. O. Ngongang Ndjawa, T. Heumueller, K. Vandewal, A. Salleo, B. F. Chmelka, A. Amassian, P. M. Beaujuge and M. D. McGehee, *Journal of the American Chemical Society*, 2014, 136, 9608-9618.

24. S. C. Natalie Banerji, Mario Leclerc, Eric Vauthey, Alan J. Heeger, *Journal of American Chemical Society*, 2010, 132, 17459-17470.
25. I. Hwang, S. Beaupré, M. Leclerc and G. D. Scholes, *Chemical Science*, 2012, 3, 2270-2277.
26. N. Banerji, E. Gagnon, P.-Y. Morgantini, S. Valouch, A. R. Mohebbi, J.-H. Seo, M. Leclerc and A. J. Heeger, *The Journal of Physical Chemistry C*, 2012, 116, 11456-11469.
27. J. Y. K. In-Wook Hwang, Shinuk Cho, Jonathan Yuen, Nelson Coates, Kwanghee Lee, Martin Heeney, Iain McCulloch, Daniel Moses, and A. J. Heeger, *The Journal of Physical Chemistry C*, 2008, 112, 7853-7857.
28. S. C. Natalie Banerji, Mario Leclerc, Eric Vauthey, and Alan J. Heeger, *Journal of the American Chemical Society*, 2010, 132, 17459-17470.
29. B. W. B. Nathan P. Wells, Marc A. Hillmyer, and David A. Blank, *The Journal of Physical Chemistry C*, 2007, 111, 15404-15414.
30. A. R. S. Kandada, S. Guarnera, F. Tassone, G. Lanzani and A. Petrozza, *Advanced Functional Materials*, 2014, 24, 3094-3099.
31. A. A. Bakulin, A. Rao, V. G. Pavelyev, P. H. van Loosdrecht, M. S. Pshenichnikov, D. Niedzialek, J. Cornil, D. Beljonne and R. H. Friend, *Science*, 2012, 335, 1340-1344.
32. G. Grancini, M. Maiuri, D. Fazzi, A. Petrozza, H. J. Egelhaaf, D. Brida, G. Cerullo and G. Lanzani, *Nature Materials*, 2013, 12, 29-33.
33. A. E. Jailaubekov, A. P. Willard, J. R. Tritsch, W. L. Chan, N. Sai, R. Gearba, L. G. Kaake, K. J. Williams, K. Leung, P. J. Rossky and X. Y. Zhu, *Nature Materials*, 2013, 12, 66-73.
34. M. N. G. Lanzani, S. De Silvestri , R. Tubino, *Chemical Physics Letters*, 1996, 251, 339-345.
35. G. L. G. Cerullo, M. Muccini, C. Taliani, and S. De Silvestri, *Physical Review Letters*, 1999, 83, 231-234.
36. P.-L. T. Boudreault, A. Najari and M. Leclerc, *Chemistry of Materials*, 2011, 23, 456-469.
37. P. C. Chow, S. Gelinas, A. Rao and R. H. Friend, *Journal of the American Chemical Society*, 2014, 136, 3424-3429.
38. F. Gao and O. Inganas, *Physical Chemistry Chemical Physics*, 2014, 16, 20291-20304.
39. S. Gelinas, A. Rao, A. Kumar, S. L. Smith, A. W. Chin, J. Clark, T. S. van der Poll, G. C. Bazan and R. H. Friend, *Science*, 2014, 343, 512-516.
40. I. Hwang and G. D. Scholes, *Chemistry of Materials*, 2011, 23, 610-620.

41. O. G. Reid, R. D. Pensack, Y. Song, G. D. Scholes and G. Rumbles, *Chemistry of Materials*, 2014, 26, 561-575.
42. B. M. Savoie, N. E. Jackson, L. X. Chen, T. J. Marks and M. A. Ratner, *Account of Chemical Research*, 2014, 47, 3385-3394.
43. J. Clark, T. Nelson, S. Tretiak, G. Cirmi and G. Lanzani, *Nature Physics*, 2012, 8, 225-231.
44. T. Nelson, S. Fernandez-Alberti, A. E. Roitberg and S. Tretiak, *Accounts of Chemical Research*, 2014, 47, 1155-1164.
45. T. Nelson, S. Fernandez-Alberti, A. E. Roitberg and S. Tretiak, *Physical Chemistry Chemical Physics*, 2013, 15, 9245-9256.
46. S. Fernandez-Alberti, V. D. Kleiman, S. Tretiak and A. E. Roitberg, *The Journal of Physical Chemistry Letters*, 2010, 1, 2699-2704.
47. N. Oldani, S. Tretiak, G. Bazan and S. Fernandez-Alberti, *Energy & Environmental Science*, 2014, 7, 1175-1184.
48. J. C. Tully, *The Journal of Chemical Physics*, 1990, 93, 1061-1071.
49. T. Nelson, S. Fernandez-Alberti, V. Chernyak, A. E. Roitberg and S. Tretiak, *The Journal of Physical Chemistry B*, 2011, 115, 5402-5414.
50. B. Habenicht, C. Craig and O. Prezhdo, *Physical Review Letters*, 2006, 96, 187401-187404.
51. B. Habenicht and O. Prezhdo, *Physical Review Letters*, 2008, 100, 197402.
52. C. Craig, W. Duncan and O. Prezhdo, *Physical Review Letters*, 2005, 95, 163001-163004.
53. J. Liu, A. J. Neukirch and O. V. Prezhdo, *The Journal of Physical Chemistry C*, 2014, 118, 20702-20709.
54. A. V. Akimov and O. V. Prezhdo, *Journal of the American Chemical Society*, 2014, 136, 1599-1608.
55. A. V. Akimov and O. V. Prezhdo, *Journal of Chemical Theory and Computation*, 2013, 9, 4959-4972.
56. R. Long, N. J. English and O. V. Prezhdo, *Journal of the American Chemical Society*, 2013, 135, 18892-18900.
57. R. Long and O. V. Prezhdo, *Nano Letters*, 2014, 14, 3335-3341.
58. H. Tamura, E. R. Bittner and I. Burghardt, *The Journal of Chemical Physics*, 2007, 127, 034706-034718.
59. R. F. M. M. Muccini, R. Hennig, U. Lemmer, H. Baessler, F. Biscarini, R. Zamboni, C. Taliani *Chemical Physics Letters*, 1995, 242, 5.
60. M. Muccini, E. Lunedei, C. Taliani, D. Beljonne, J. Cornil and J. L. Brédas, *The Journal of Chemical Physics*, 1998, 109, 10513-10520.

61. J.-P. C. Jérôme Cornil, David Beljonne, Robert Silbey, and Jean-Luc Brédas, *Advanced Materials*, 2000, 12, 978-983.
62. K. Sen, R. Crespo-Otero, O. Weingart, W. Thiel and M. Barbatti, *Journal of Chemical Theory and Computation*, 2013, 9, 533-542.
63. R. Crespo-Otero and M. Barbatti, *Theoretical Chemistry Accounts*, 2012, 131, 1237.
64. J. D. Chai and M. Head-Gordon, *Physical Chemistry Chemical Physics*, 2008, 10, 6615-6620.
65. F. J. D. P. J. Stephens, C. F. Chabalowski, M. J. Frisch, *Journal of Physical Chemistry* 1994, 98, 11623-11627.
66. A. D. Becke, *The Journal of Chemical Physics*, 1993, 98, 5648-5652.
67. C. Adamo and V. Barone, *The Journal of Chemical Physics*, 1999, 110, 6158.
68. T. Yanai, D. P. Tew and N. C. Handy, *Chemical Physics Letters*, 2004, 393, 51-57.
69. B. F. Curchod, U. Rothlisberger and I. Tavernelli, *Chemphyschem : a European journal of chemical physics and physical chemistry*, 2013, 14, 1314-1340.
70. M. Barbatti, *Wiley Interdisciplinary Reviews: Computational Molecular Science*, 2011, 1, 620-633.
71. E. Fabiano, T. W. Keal and W. Thiel, *Chemical Physics*, 2008, 349, 334-347.
72. M. Barbatti, G. Granucci, M. Persico, M. Ruckenbauer, M. Vazdar, M. Eckert-Maksić and H. Lischka, *Journal of Photochemistry and Photobiology A: Chemistry*, 2007, 190, 228-240.
73. M. Barbatti, M. Ruckenbauer, F. Plasser, J. Pittner, G. Granucci, M. Persico and H. Lischka, *Wiley Interdisciplinary Reviews: Computational Molecular Science*, 2014, 4, 26-33.
74. M. J. Frisch, G. W. Trucks, H. B. Schlegel, G. E. Scuseria, M. A. Robb, J. R. Cheeseman, G. Scalmani, V. Barone, B. Mennucci, G. A. Petersson, H. Nakatsuji, M. Caricato, X. Li, H. P. Hratchian, A. F. Izmaylov, J. Bloino, G. Zheng, J. L. Sonnenberg, M. Hada, M. Ehara, K. Toyota, R. Fukuda, J. Hasegawa, M. Ishida, T. Nakajima, Y. Honda, O. Kitao, H. Nakai, T. Vreven, J. A. Montgomery Jr., J. E. Peralta, F. Ogliaro, M. J. Bearpark, J. Heyd, E. N. Brothers, K. N. Kudin, V. N. Staroverov, R. Kobayashi, J. Normand, K. Raghavachari, A. P. Rendell, J. C. Burant, S. S. Iyengar, J. Tomasi, M. Cossi, N. Rega, N. J. Millam, M. Klene, J. E. Knox, J. B. Cross, V. Bakken, C. Adamo, J. Jaramillo, R. Gomperts, R. E. Stratmann, O. Yazyev, A. J. Austin, R. Cammi, C. Pomelli, J. W. Ochterski, R. L. Martin, K. Morokuma, V. G. Zakrzewski, G. A. Voth, P. Salvador, J. J. Dannenberg, S. Dapprich, A. D. Daniels, Ö. Farkas, J. B. Foresman, J. V. Ortiz, J. Cioslowski and D. J. Fox, Gaussian, Inc., Wallingford, CT, USA, 2009.

75. G. Granucci and M. Persico, *The Journal of Chemical Physics*, 2007, 126, 134114-134123.
76. S. Hammes-Schiffer and J. C. Tully, *The Journal of Chemical Physics*, 1994, 101, 4657-4667.
77. M. Barbatti, J. Pittner, M. Pederzoli, U. Werner, R. Mitrić, V. Bonačić-Koutecký and H. Lischka, *Chemical Physics*, 2010, 375, 26-34.
78. F. Plasser, R. Crespo-Otero, M. Pederzoli, J. Pittner, H. Lischka and M. Barbatti, *Journal of Chemical Theory and Computation*, 2014, 10, 1395-1405.
79. M. Barbatti, *Journal of the American Chemical Society*, 2014, 136, 10246-10249.
80. TURBOMOLE V6.3 2011, a development of University of Karlsruhe and Forschungszentrum Karlsruhe GmbH, 1989-2007, and TURBOMOLE GmbH, since 2007; available from: http://www.turbomole.com.
81. N. Gavrilov, S. Salzmann and C. M. Marian, *Chemical Physics*, 2008, 349, 269-277.
82. S. Salzmann, M. Kleinschmidt, J. Tatchen, R. Weinkauf and C. M. Marian, *Physical Chemistry Chemical Physics*, 2008, 10, 380-392.
83. R. Weinkauf, L. Lehr, E. W. Schlag, S. Salzmann and C. M. Marian, *Physical Chemistry Chemical Physics*, 2008, 10, 393-404.
84. S. Siegert, F. Vogeler, C. M. Marian and R. Weinkauf, *Physical Chemistry Chemical Physics*, 2011, 13, 10350-10363.
85. M. Stenrup, *Chemical Physics*, 2012, 397, 18-25.
86. G. Cui and W. Fang, *The Journal of Physical Chemistry A*, 2011, 115, 11544-11550.
87. I. C. W. Michael H. Palmer, Martyn F. Guest, *Chemical Physics*, 1999, 241, 275-296.
88. U. Salzner and A. Aydin, *Journal of Chemical Theory and Computation*, 2011, 7, 2568-2583.
89. U. Salzner, *J Chem Theory Comput*, 2007, 3, 1143-1157.
90. M. H. D. Grebner, and S. Rentsch, *J Phys Chem*, 1995, 99, 16991-16998.
91. D. G. R. Colditz, M. Helbig, S. Rentsch, *Chemical Phyics*, 1995, 201, 309-320.
92. J. S. d. M. Ralph S. Becker, António L. Mac ̧anita, and Fausto Elisei, *The Journal of Chemical Physics*, 1996, 100, 18683-18695.
93. J. Seixas de Melo, H. D. Burrows, M. Svensson, M. R. Andersson and A. P. Monkman, *The Journal of Chemical Physics*, 2003, 118, 1550-1556.
94. F. C. Spano, *Annual Review of Physical Chemistry*, 2006, 57, 217-243.
95. S. Schols, C. McClatchey, C. Rolin, D. Bode, J. Genoe, P. Heremans and A. Facchetti, *Advanced Functional Materials*, 2008, 18, 3645-3652.
96. E. Stendardo, F. Avila Ferrer, F. Santoro and R. Improta, *Journal of Chemical Theory and Computation*, 2012, 8, 4483-4493.

97. J. Casado, R. Ponce Ortiz and J. T. Lopez Navarrete, *Chemical Society Reviews*, 2012, 41, 5672-5686.

98. N. Z. Sanjio S. Zade, and Michael Bendikov, *Account of Chemical Research*, 2010, 44, 14-24.

99. C. A. Rozzi, S. M. Falke, N. Spallanzani, A. Rubio, E. Molinari, D. Brida, M. Maiuri, G. Cerullo, H. Schramm, J. Christoffers and C. Lienau, *Nature Communications*, 2013, 4, 1602-1608.

Table of Contents (TOC) Image

Nonadiabatic excited-state dynamics reveal the exciton relaxation processes in oligothiophenes. Ultrafast deactivation and exciton localization are predicted to occur within 200 fs, involving bond stretching, ring puckering, and torsional oscillations.